Springer

Journal of Mechanical Science and Technology 22 (2008) 2030~2037

Journal of Mechanical Science and Technology

www.springerlink.com/content/1738-494x
DOI 10.1007/s12206-008-0752-7

The effect of additional equilibrium stress functions on the three-node hybrid-mixed curved beam element †

Jin-Gon Kim* and Yong Kuk Park

School of Mechanical and Automotive Engineering, Catholic University of Daegu, Hayang-Eup, Gyeongsan-si, Gyeongbuk, 712-702, Korea

(Manuscript Received December 14, 2007; Revised June 5, 2008; Accepted July 31, 2008)

Abstract

To develop an effective hybrid-mixed element, it is extremely critical as to how to assume the stress field. This research article demonstrates the effect of additional equilibrium stress functions to enhance the numerical performance of the locking-free three-node hybrid-mixed curved beam element, proposed in Saleeb and Chang's previous work. It is exceedingly complicated or even infeasible to determine the stress functions to satisfy fully both the equilibrium conditions and suppression of kinematic deformation modes in the three-node hybrid-mixed formulation. Accordingly, the additional stress functions to satisfy partially or fully equilibrium conditions are incorporated in this study. Several numerical examples for static and dynamic problems confirm that the newly proposed element with these additional stress functions is highly effective regardless of the slenderness ratio and curvature of arches in static and dynamic analyses.

Keywords: Three-noded curved beam element; Hybrid-mixed formulation; Additional equilibrium stress functions; Field-consistency

1. Introduction

Curved beam elements have been the subject of intensive research interest to gain insight into more complex behaviors of shell problems. Due to the numerical problems, such as the locking phenomena and severe disturbance of stress prediction in the earliest attempts, numerous noteworthy elements based on the minimum potential energy principle have been proposed [1-9]. As an alternative to these displacement-based elements, considerable efforts have been devoted to the development of mixed or hybrid-mixed finite elements [10-15]. Among these, Saleeb and Chang [11] developed well-known two-node and three-node C^0 curved beam elements that satisfy two significant considerations in selecting the stress functions. However, these elements proved not to show superior numerical behaviors to existing elements. Zhang [12] demonstrated that Saleeb and Chang's hybrid-mixed curved beam elements are identical to reduced integration elements from a different point of view. Dorfi and Busby [13] introduced a two-node hybrid-mixed laminated composite curved beam element. Lastly, Kim et al. [14, 15] enhanced the numerical performance of a two-node hybrid-mixed linear element by employing the nodeless internal degrees of freedom in interpolating the displacement field and field-consistent stress functions. However, additional computational efforts were inevitable to construct the stiffness and mass matrix of a conventional size.

The objective of this research paper is to display the effect of the additional stress functions in a stress field to satisfy partially or fully equilibrium conditions on the development of effective three-node hybrid-mixed curved beam elements. For this purpose,

† This paper was recommended for publication in revised form by Associate Editor Maenghyo Cho

*Corresponding author. Tel.: +82 53 850 2711, Fax.: +82 53 850 2710
E-mail address: kimjg1@cu.ac.kr

Saleeb and Chang's HMC3 element is considered as a reference model. The proposed elements do not require additional computational efforts via the usual Lagrangian quadratic interpolation functions to assume the displacements. Several numerical examples will confirm that these additional stress functions are highly efficacious in improving the numerical stability and convergence without regard for the slenderness ratio of arches and curvature.

2. Hybrid-mixed formulation

Fig. 1 shows the geometry of a three-node curved beam element having the thickness h, beam width b, initial radius of curvature R and length $l = R\varphi_0$. By employing Hamilton's principle, the equations of motion can be derived as:

$$\delta H = \delta \int_{t_0}^{t_1} (\Pi_{HR} - T)\,\mathrm{d}t = 0 \tag{1}$$

where Π_{HR} and T are the Hellinger-Reissner functional and the kinetic energy, respectively, given by

$$\Pi_{HR} = \int_c (\boldsymbol{\sigma}^T \boldsymbol{\varepsilon} - \frac{1}{2}\boldsymbol{\sigma}^T \mathbf{S}\boldsymbol{\sigma})\,\mathrm{d}x - W\,;$$
$$T = \frac{1}{2}\int_c \rho\, \dot{\mathbf{u}}^T \boldsymbol{\Lambda} \dot{\mathbf{u}}\,\mathrm{d}x \tag{2}$$

and

$$W = \int_c (p_x u + p_y v)\,dx + \sum_{i=1}^{3} \left(N_i u_i + V_i v_i + M_i \theta_i\right) \tag{3a}$$

$$\boldsymbol{\Lambda} = \begin{bmatrix} \rho A & 0 & 0 \\ 0 & \rho A & 0 \\ 0 & 0 & \rho I \end{bmatrix}. \tag{3b}$$

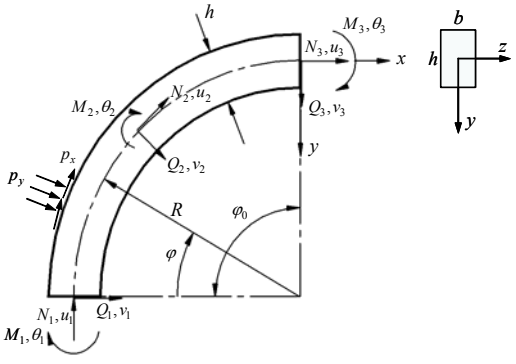

Fig. 1. Geometry of a three-noded curved beam element.

where $\boldsymbol{\sigma} = [N, V, M]^T$ are generalized stress resultants, $\boldsymbol{\varepsilon} = [\varepsilon_0, \gamma_0, \kappa]^T$ are generalized strains, $\mathbf{u} = [u, v, \theta]^T$ are displacements, ρ is the mass density, and the dots denote derivatives with respect to time t. The stress resultants $\boldsymbol{\sigma}$ and strains $\boldsymbol{\varepsilon}$ have the relation as $\boldsymbol{\varepsilon} = \mathbf{S} \cdot \boldsymbol{\sigma}$, where $\mathbf{S}$ is a generalized material compliance matrix. From the general equations of the higher-order approximation theory by Naghdi and Reissner [16] for shells, the curved beam theory is derived as

$$\begin{Bmatrix} \varepsilon_0 \\ \gamma_0 \\ \kappa \end{Bmatrix} = \begin{bmatrix} \frac{1}{R}\frac{d}{d\varphi} & -\frac{1}{R} & 0 \\ \frac{1}{R} & \frac{1}{R}\frac{d}{d\varphi} & -1 \\ 0 & 0 & \frac{1}{R}\frac{d}{d\varphi} \end{bmatrix} \begin{Bmatrix} u \\ v \\ \theta \end{Bmatrix} \tag{4a}$$

$$\begin{Bmatrix} N \\ V \\ M \end{Bmatrix} = EA \begin{bmatrix} 1 + \frac{I}{AR^2} & 0 & \frac{I}{AR} \\ 0 & \frac{kG}{E} & 0 \\ \frac{I}{AR} & 0 & -\frac{I}{A} \end{bmatrix} \begin{Bmatrix} \varepsilon_0 \\ \gamma_0 \\ \kappa \end{Bmatrix} \tag{4b}$$

where E is the elastic modulus, G is the shear modulus, k is the shear correction factor, and A and I are the area and moment of inertia of the cross-section, respectively. For a rectangular cross-section, Roark [17] calculates $k = 5/6$ by means of the elementary strain-energy method, and Cowper [18] derives $k = (10 + 10\nu)/(12 + 11\nu)$ depending on Poisson's ratio.

The three equilibrium conditions for a curved beam element displayed in Fig. 1 are given by

$$\frac{1}{R}\frac{dN}{d\varphi} - \frac{V}{R} + p_x = 0\,;\quad \frac{1}{R}\frac{dV}{d\varphi} + \frac{N}{R} + p_y = 0\,;$$
$$\frac{1}{R}\frac{dM}{d\varphi} + V = 0 \tag{5}$$

For finite element approximations, the displacements and stress resultants are independently interpolated in terms of nodal displacement, $\mathbf{d}$, and stress parameters, $\boldsymbol{\beta}$, as

$$\mathbf{u} = \mathbf{N} \cdot \mathbf{d}\ ;\quad \boldsymbol{\sigma} = \mathbf{P} \cdot \boldsymbol{\beta} \tag{6}$$

where $\mathbf{N}$ and $\mathbf{P}$ are the matrices of interpolation functions for element displacements and generalized

stresses, respectively. Combination of Eqs. (1), (2) and (6) yields

$$H = \boldsymbol{\beta}^T\mathbf{G}\mathbf{d} - \frac{1}{2}\boldsymbol{\beta}^T\mathbf{H}\boldsymbol{\beta} - \mathbf{d}^T\boldsymbol{\Phi} - \mathbf{Q}^T\mathbf{d} - \frac{1}{2}\omega^2\mathbf{d}^T\mathbf{M}\mathbf{d} \quad (7)$$

where

$$\mathbf{H} = \int_c \mathbf{P}^T\mathbf{S}\mathbf{P}\mathrm{d}x \;\; ; \;\; \mathbf{G} = \int_c \mathbf{P}^T\boldsymbol{\Delta}\mathbf{N}\mathrm{d}x \quad (8a)$$

$$\boldsymbol{\Phi} = \int_c \mathbf{N}^T\left[p_x, p_y, 0\right]^T \mathrm{d}x \;\; ; \;\; \mathbf{M} = \int_c \mathbf{N}^T\boldsymbol{\Lambda}\mathbf{N}\mathrm{d}x \quad (8b)$$

and $\mathbf{Q}$ is an equivalent nodal force vector, and $\mathbf{M}$ is a consistent element mass matrix.

Invoking the stationarity of Eq. (7) with respect to $\mathbf{d}$ and $\boldsymbol{\beta}$, respectively, and then the substituting the stress resultant parameters $\boldsymbol{\beta}$ for nodal displacements $\mathbf{d}$ on the element level yield

$$[\mathbf{K} - \omega^2\mathbf{M}]\cdot\mathbf{d} = \mathbf{Q} + \boldsymbol{\Phi} \quad (9)$$

where the element stiffness matrix $\mathbf{K}$ is expressed as

$$\mathbf{K} = \mathbf{G}^T\mathbf{H}^{-1}\mathbf{G} \; . \quad (10)$$

3. Field assumptions

For three-node hybrid-mixed curved beam elements, the usual Lagrangian interpolation functions are used to assume the displacements in Eq. (2). Using the dimensionless co-ordinate $\xi = \varphi/\varphi_0 = x/l$ $(0 \le \xi \le 1)$, the displacements are assumed as

$$u = \sum_{k=1}^{3} N_k u_k \; ; \;\; v = \sum_{k=1}^{3} N_k v_k \; ; \;\; \theta = \sum_{k=1}^{3} N_k \theta_k \quad (11)$$

where

$$N_1 = 1 - 3\xi + 2\xi^2 \; ; \;\; N_2 = 2\xi^2 - \xi \; ; \;\; N_3 = 4\xi(1-\xi) \quad (12)$$

and $\mathbf{d} = \{u_k, v_k, \theta_k\}_{k=1,2,3}$ are the nodal displacement degrees of freedom.

Saleeb and Chang [11] assumed the following field-consistent linear stress functions in Eq. (13). All the kinematic deformation modes are suppressed, and the spurious constraints are removed in the inextensional bending limit behavior and Kirchhoff limit behavior in very thin and nearly straight beams.

$$\mathbf{P} = \begin{bmatrix} 1 & 0 & 0 & \xi & 0 & 0 \\ 0 & 1 & 0 & 0 & \xi & 0 \\ 0 & 0 & 1 & 0 & 0 & \xi \end{bmatrix} \quad (13)$$

In the context of present three-node curved beam elements, several attempts for assuming stress resultants are made to study the effect of additional stress functions to satisfy partially or fully homogeneous equilibrium conditions in assuming stress field on the numerical performance of Saleeb and Chang's three-node element, HMC3.

3.1 Additional equilibrium stress functions model 1 (designated as EMC3a)

When the moment-shear force equilibrium equation in Eq. (5)

$$\frac{dM}{ld\xi} = -V = -\beta_2 - \beta_5\xi \quad (14)$$

is taken into consideration, the following stress functions can be added in the moment resultant in Eq. (13) as

$$\mathbf{P} = \begin{bmatrix} 1 & 0 & 0 & \xi & 0 & 0 \\ 0 & 1 & 0 & 0 & \xi & 0 \\ 0 & -l\xi & 1 & 0 & -l\xi^2/2 & \xi \end{bmatrix}. \quad (15)$$

These stress functions produce the membrane strain in the extensional bending limit behavior as

$$\begin{aligned} \varepsilon_0 &= \frac{1}{AE}(N + \frac{M}{R}) \\ &= \frac{1}{AE}[(\beta_1 + \frac{1}{R}\beta_3) + (\beta_4 - \frac{l}{R}\beta_2 + \frac{1}{R}\beta_6)\xi \\ &\quad - \frac{l}{2R}\beta_5\xi^2] \to 0 \end{aligned} \quad (16)$$

We can apprehend that the spurious constraint cannot be excluded indirectly in this field-inconsistent m embrane strain due to second-order term.

3.2 Relaxed equilibrium stress functions model 2 (designated as EMC3b)

When the shear force-axial force and moment-shear force homogeneous equilibrium in Eq. (5) are considered, the coupled conditions can be obtained as

$$\frac{d^2M}{d\xi^2}=\frac{1}{R}N\ ;\ \frac{dM}{ld\xi}=-V \tag{17}$$

These two coupled equations yield the following added stress functions in the moment resultant as

$$\mathbf{P}=\begin{bmatrix} 1 & 0 & 0 & \xi & 0 & 0 \\ 0 & 1 & 0 & 0 & \xi & 0 \\ (l\xi)^2/(2R) & -l\xi & 1 & l^2\xi^3/(6R) & -l\xi^2/2 & \xi \end{bmatrix}. \tag{18}$$

These stress functions yield the membrane strain in the extensional bending limit behavior as

$$\begin{aligned}\varepsilon_0=\frac{1}{AE}[&(\beta_1+\frac{1}{R}\beta_3)+(\beta_4-\frac{l}{R}\beta_2+\frac{1}{R}\beta_6)\xi \\ &+(\frac{l^2}{2}\beta_1-\frac{l}{2R}\beta_5)\xi^2+\frac{l^2}{6}\beta_4\xi^3]\to 0\end{aligned} \tag{19}$$

and the third-order term to produce a spurious constraint makes this membrane strain field-inconsistent.

3.3 Relaxed equilibrium stress functions model 3 (designated as EMC3c)

When considering Eq. (5), the homogeneous linear differential equation can be derived as

$$\frac{d^2N}{d\varphi^2}+N=0 \tag{20}$$

Solving this differential equation, we can obtain the following stress functions to satisfy all the homogeneous equilibrium equations in Eq. (5) as

$$N=\cos\varphi\beta_1+\sin\varphi\beta_2 \tag{21a}$$
$$V=-\sin\varphi\beta_1+\cos\varphi\beta_2 \tag{21b}$$
$$M=-R(\cos\varphi-1)\beta_1-R\sin\varphi\beta_2+\beta_3 \tag{21c}$$

In a nearly straight beam ($\varphi\to 0$), these stress functions become

$$N=\beta_1\ ;\ V=\beta_2\ ;\ M=\beta_3 \tag{22}$$

and these are identical to the stress parameters in Saleeb and Chang's two-node HMC2 element. To satisfy the Pian and Chen's guidelines [19] and the field-consistency in the limit behaviors, the following supplementary stress functions are added to Eq. (13).

$$\mathbf{P}=\begin{bmatrix} \cos\varphi & \sin\varphi & 0 & \xi & 0 & 0 \\ -\sin\varphi & \cos\varphi & 0 & 0 & \xi & 0 \\ -R(\cos\varphi-1) & -R\sin\varphi & 1 & 0 & 0 & \xi \end{bmatrix} \tag{23}$$

These stress functions, becoming identical to those of HMC3 element in a nearly straight beam, have no spurious constraints in Kirchhoff limit behavior. Besides, we can easily confirm that the spurious constraint in the inextensional bending limit is removed in the following form of membrane strain:

$$\varepsilon_0=\frac{1}{AE}[(\beta_1+\frac{1}{R}\beta_3)+(\beta_4+\frac{1}{R}\beta_6)\xi]\to 0\,. \tag{24}$$

3.4 Inconsistent stress functions model (designated as IHMC3)

To examine the effect of the field-consistent stress parameters on a three-node hybrid-mixed formulation, the following quadratic stress functions with the field-inconsistent terms will be considered.

$$\mathbf{P}=\begin{bmatrix} 1 & 0 & 0 & \xi & 0 & 0 & \xi^2 & 0 & 0 \\ 0 & 1 & 0 & 0 & \xi & 0 & 0 & \xi^2 & 0 \\ 0 & 0 & 1 & 0 & 0 & \xi & 0 & 0 & \xi^2 \end{bmatrix} \tag{25}$$

4. Results and discussions

To demonstrate the effect of the proposed additional equilibrium functions on the performance of three-node hybrid-mixed elements, several static and dynamic numerical examples are considered in terms of locking phenomena, convergence, and stress predictions. The numerical values of geometrical dimensions and material properties given for the numerical examples are in consistent units. Shear correction factor $k=5/6$, elastic modulus $E=10.5\times10^6$, Poisson's ratio $\nu=0.3125$, and shear modulus $G=0.5E/(1+\nu)$ are applied throughout the analysis. All calculations are carried out by using MATLAB.

4.1 Cantilever circular arch

A cantilever circular arch subjected to a radial point load $P=1$ at the free end is considered to check the effect of shear and membrane locking. Fig. 2 shows the tip deflection in a nearly straight cantilever arch with $L=10$ and $R=10^5$, which is normalized by the following exact solution derived from Castigli-

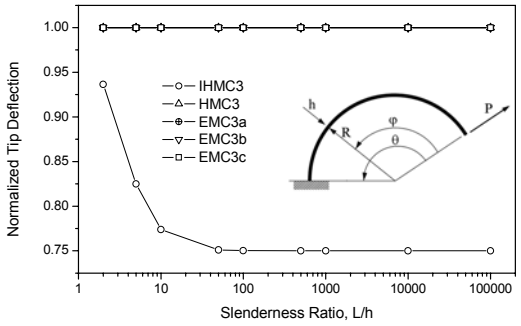

Fig. 2. Shear locking test for the tip deflection normalized by the exact solution using one element in a nearly straight cantilever beam with unit width $b=1$ and subtended angle $\theta=0^{\circ}$.

ano's theorem, over the entire range of slenderness ratio, $L/h=2$ to 10^5.

$$v_{tip}=\frac{PR^3\theta}{2EI}\left[1+\frac{I}{AR^2}\left(1+\frac{2(1+\nu)}{k}\right)\right]+\frac{PR^3\sin 2\theta}{4EI}\left[\frac{I}{AR^2}\left(\frac{2(1+\nu)}{k}-1\right)-1\right] \tag{26}$$

The finite element results for radial tip deflection at the loaded point are obtained by one-element discretization over a wide range of subtended angles and slenderness ratio. The inconsistent hybrid-mixed element IHMC3 suffers from some shear locking. However, all the proposed hybrid-mixed elements EMC3a, EMC3b, and EMCc as well as Saleeb and Chang's HMC3 element exhibit identical locking-free results even in extremely thin beams.

In addition to the shear locking test, the membrane locking phenomena appearing in thin arches are examined in Fig. 3 for the subtended angle $\theta=90^{\circ}$ over the slenderness ratios from $R/h=2$ to 10^5. The results show that IHMC has a serious membrane locking problem in thin arches. On the other hand, we can observe that present hybrid-mixed elements EMC3a, EMC3b and EMC3c are free from membrane locking problems. Fig. 4 shows the numerical stability of present hybrid-mixed elements, which have the slenderness ratio $R/h=1000$, according to the variance of curvature. EMC3b produces more accurate results than HMC3 in subtended angles less than 120°, and HMC3's error grows larger as the subtended angle becomes larger. It can be confirmed that EMC3c produces far superior stabilized results to HMC3, EMC3a, and EMC3b elements.

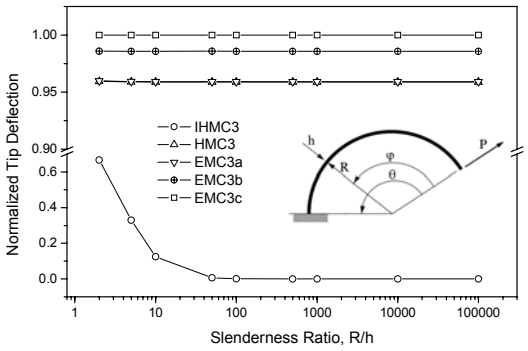

Fig. 3. Membrane locking test for the tip deflection normalized by the exact solution using one element in a moderately deep cantilever circular arch with unit width $b=1$ and subtended angle $\theta=90^{\circ}$.

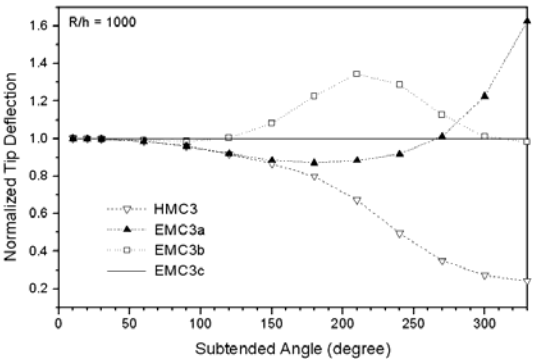

Fig. 4. Tip deflection at loaded point normalized by the exact solution over a wide range of subtended angle θ.

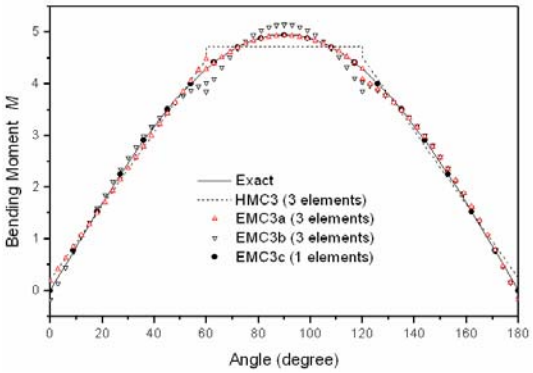

Fig. 5. Bending moment distribution of a cantilever circular arch with subtended angle $\theta=180^{\circ}$ and slenderness ratio $R/h=50$.

Fig. 5 shows the bending moment distribution of a cantilever circular arch. It is observed that the results calculated by one EMC3c agree much better with the exact solutions than those by other hybrid-mixed

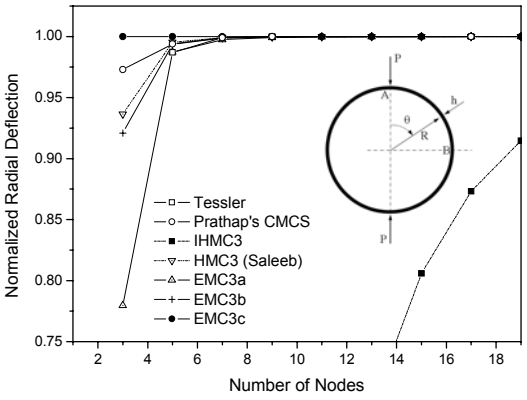

Fig. 6. Convergence trend of the normalized radial displacement at the loaded point A in a pinched ring ($R = 4.953$, $h = 0.094$, $P = 100$).

elements using three elements.

4.2 A pinched ring

Fig. 6 shows the convergence trend of the normalized radial displacement at the loaded point A in a pinched ring. Due to the double symmetry, a quadrant AB of the ring can be modeled with appropriate symmetric boundary conditions. The proposed EMC3c element yields more rapidly converging results than other elements including Prathap and Babu's CMCS element [3], Tessler's anisoparametric element [4], and Saleeb and Chang's HMC3 element [11]. Unlike the previous cantilever circular arch problem, EMC3a and EMC3b elements show a little worse convergence than HMC3 element.

4.3 Free vibration of hinged arches

The hinged arches with subtended angle α shown in Fig. 7 are considered to examine the numerical performance of the proposed elements in free vibration analyses. Figs. 8 and 9 show the locking studies for the hinged arches with $\alpha = 10^\circ$ and $\alpha = 300^\circ$ from the slenderness ratio $R/h = 5$ to $R/h = 10^6$, respectively. It can be seen that IHMC3 suffers from a severe locking problem and HMC3 yields inferior results to EMC3c in thinner and deeper hinged arches. Figs. 10 and 11 show the convergence trend of the normalized fundamental frequency for the hinged arches with $R/h = 5$ and $R/h = 1000$, respectively. Also, both HMC3 and EMC3b show unsettled convergence trends as a subtended angle becomes large. However, EMC3c has a remarkably stable conver

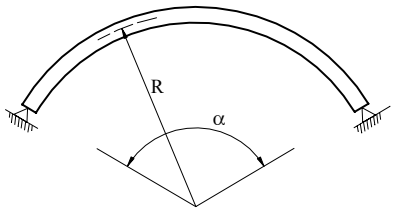

Fig. 7. A hinged arch.

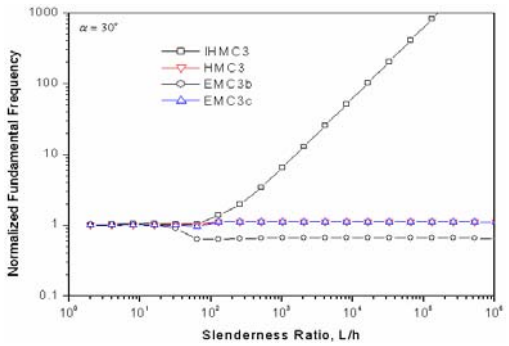

Fig. 8. Locking studies for the hinged circular arches with $\alpha = 30^\circ$.

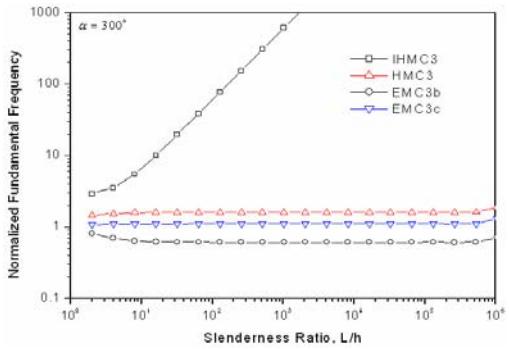

Fig. 9. Locking studies for the hinged circular arches with $\alpha = 300^\circ$.

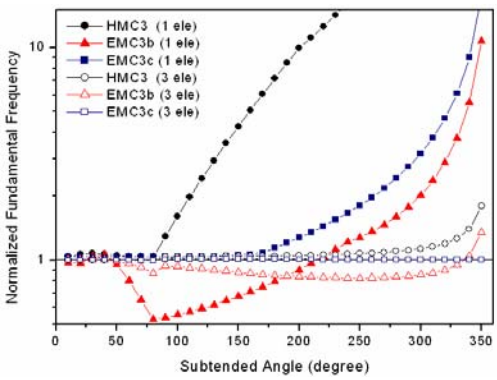

Fig. 10. Convergence trend of the normalized fundamental frequency for the hinged circular arches with $R/h = 5$.

Table 1. Fundamental frequencies (rad/s) for hinged circular arches computed by present three-noded hybrid-mixed elements($R=12$; $E=3.04\times10^{7}$; $\nu=0.3$; $\rho=0.02736$; $A=0.1563\ \text{in}^2$; $I=8.138\times10^{-4}$; $k=0.8497$; $h=0.25$).

Angles (degree)	IHMC3 (21 d.o.f.)	HMC3 (21 d.o.f.)	EMC3c (21 d.o.f.)	Leung's THICK-2	Krishnan's E1.1b (84 d.o.f.)	Heppler (27 d.o.f.)
10	5910.7	5842.3	5842.0	5841.74	5874.3	5849.9
20	2849.8	2827.7	2826.5	2827.63	2823.1	2830.2
30	2548.1	2418.5	2342.8	2339.82	2345.2	2339.7
60	840.85	579.67	561.92	560.25	561.2	560.24
90	559.46	237.93	230.75	229.66	230.4	229.77
120	474.77	120.06	116.18	115.64	116.3	115.64
150	425.04	67.12	64.72	64.43	64.93	64.44
180	384.61	39.63	38.02	37.86	38.24	37.87
210	348.74	24.01	22.86	22.77	23.05	22.77
240	316.44	14.58	13.72	13.66	13.87	13.67
270	287.43	8.62	7.95	7.92	8.06	7.93
300	261.45	4.74	4.20	4.18	4.27	4.19
330	238.25	2.14	1.70	1.69	1.73	1.69
350	224.20	0.89	0.50	0.49	0.50	0.24

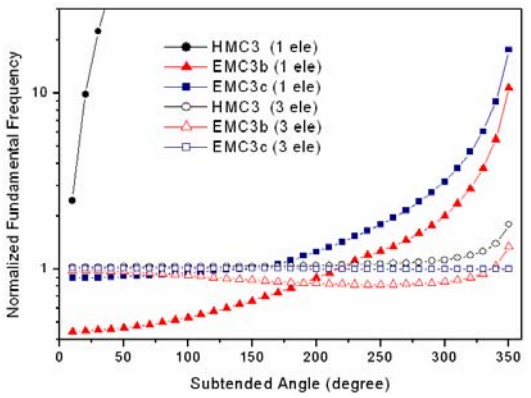

Fig. 11. Convergence trend of the normalized fundamental frequency for the hinged circular arches with $R/h=1000$.

gence in a free vibration analysis regardless of the slenderness ratio and subtended angle. In a free vibration problem, it can be confirmed repeatedly that the hybrid-mixed element EMC3c with the additional equilibrium stress functions shows a superior and robust behavior for the entire range of slenderness ratio and subtended angle.

The numerical results by considered hybrid-mixed elements IHMC3, HMC3 and EMC3c using three-element idealization (21 d.o.f.) are listed in Table 1. A comparison with other existing numerical results [8, 20, 21] is carried out. Each number in parentheses is the number of total d.o.f. used in the vibration analysis. The proposed ECM3 element shows a far superior agreement with Leung and Zhu's Fourier *p*-element THICK-2 [8] and Krishnan's E1.1*b* element [21] all over the range of subtended angle to IHMC3 and HMC3 elements. Although the inconsistent hybrid-mixed element IHMC3 uses higher-order interpolation functions than the consistent hybrid-mixed element HMC3, the HMC3 element generates more converging results than the IHMC3 element, especially for a larger subtended angle. This result evidently shows that the well-established consistent stress functions are greatly important in hybrid-mixed formulation for curved beam vibrations.

5. Conclusions

We examined the effect of additional stress functions to satisfy partially or fully equilibrium conditions on the three-node hybrid-mixed curved beam element. For this objective, Saleeb and Chang's HMC3 element was considered as our reference model. The proposed hybrid-mixed elements, EMC3a and EMC3b yield sensitive results to the curvature of arches due to their field-inconsistency in membrane strain, despite the introduction of additional equilibrium stress functions. Several numerical examples confirm that the proposed EMC3c element with the field-consistent additional equilibrium stress functions produces highly accurate and stabilized results, regardless of curvature and slenderness ratio of arches in static and dynamic analyses. Especially, EMC3c element demonstrates a superb ability in predicting stress resultant distributions.

References

[1] A. K. Noor and J. M. Peters, Mixed models and reduced/selective integration displacement models for nonlinear analysis of curved beams, *International Journal for Numerical Methods in Engineering*, 17 (1981) 615-631.

[2] H. Stolarski and T. Belytschko, Membrane locking and reduced integration for curved beams, *Journal of Applied Mechanics*, 49 (1982) 172-176.

[3] G. Prathap and C. R. Babu 1986, An isoparametric 1uadratic thick curved beam element, *International Journal for Numerical Methods in Engineering*, 23 (1986) 1583-1600.

[4] A. Tessler and L. Spiridigliozzi, Curved beam elements with penalty relaxation, *International Journal for Numerical Methods in Engineering*, 23

(1986) 2245-2262.
[5] H. S. Ryu and H. C. Sin, Curved beam elements based on strain fields, *Communications in Numerical Methods in Engineering*, 12 (1986) 767-773.
[6] P. Raveendranath, G. Singh and B. Pradhan Free vibration of arches using a curved beam element based on a coupled polynomial eisplacement field, *Computers and Structures*, 78 (2000) 583-590.
[7] J. H. Lee, In-plane free vibration analysis of curved Timoshenko beams by the pseudospectral method, *KSME International Journal*, 17 (8) (2003) 1156-1163.
[8] A. Y. T. Leung and B. Zhu, Fourier p-elements for curved beam vibrations, *Thin-Walled Structures*, 42 (2004) 39-57.
[9] C. B. Kim, J. W. Park, S. H. Kim and C. D. Cho, A finite thin circular beam element for in-plane vibration analysis of curved beams, *Journal of Mechanical Science and Technology*, 19 (2005) 2187-2196.
[10] M.Gellert and M. E. Laursen, Formulation and convergence of a mixed finite element method applied to elastic arches of arbitrary geometry and loading, *Computer Methods in Applied Mechanics and Engineering*, 7 (1976) 285-302.
[11] A. F. Saleeb and T. Y. Chang, On the hybrid-mixed formulation C^0 curved beam elements, *Computer Methods in Applied Mechanics and Engineering*, 60 (1987) 95-121.
[12] Z. Zhang, A note on the hybrid-mixed C^0 curved beam elements, *Computer Methods in Applied Mechanics and Engineering*, 95 (1992) 243-252.
[13] H. R. Dorfi and H. R. Busby An effective curved composite beam finite element based on the hybrid-mixed formulation, *Computers and Structures*, 53 (1994) 43-52.
[14] J. G. Kim and Y. Y. Kim, A new higher-order hybrid-mixd curved beam element, *International Journal for Numerical Methods in Engineering*, 43 (1998) 925-940.
[15] J. G. Kim and Y. K. Park, Hybrid-mixed curved beam elements with increased degrees of freedom for static and vibration analyses, *International Journal for Numerical Methods in Engineering*, 683 (2006) 6905-706.
[16] H. Kraus, *Thin Elastic Shells*, Wiely, New York, USA, (1967).
[17] T. Kaneko, On Timoshenko's correction for shear in vibrating beams, *Journal of Physics D: Applied Physics*, 8 (1975) 1927-1936.?
[18] G. R. Cowper, The shear coefficient in Timoshenko's beam theory, *Journal of Applied Mechanics*, 33 (1966) 335-340.
[19] T. H. H. Pian and D. P. Chen Alternative ways for formulation of hybrid-stress elements, *International Journal of Solids and Structures*, 18 (1982) 1679-1684.
[20] G. R. Heppler, An element for studying the vibration of unrestrained curved Timoshenko beams, *Journal of Sound and Vibration*, 158 (1992) 387-404.
[21] A. Krishnan and H. C. Suresh, A simple cubic linear element for static and free vibration analyses of curved beams, *Computers and Structures*, 68 (1998) 473-489.

Jin-Gon Kim graduated from the Seoul National University in 1991, majoring in Mechanical Engineering. He received Master's degree and Ph.D. degree in Mechanical Engineering at the Seoul National University in 1993 and 1998, respectively. He has worked for Samsung Electronics for three years from March 1998 to February 2001, and is currently in the School of Mechanical and Automotive Engineering at Catholic University of Daegu. Main research interests include structural/impact anlyses, advanced finite element method and CAE.

Yong Kuk Park graduated from the Seoul National University in 1987, majoring in Metallurgical Engineering. He received Master's degree in Industrial and Systems Engineering at the University of Michigan in 1988, and Ph.D. degree in Manufacturing Engineering at the Ohio State University in 1995. He has worked for Samsung Motor Co., and is currently in the School of Mechanical and Automotive Engineering at Catholic University of Daegu, teaching Manufacturing Design, Statistical Quality Control, Casting and Plasticity, Forging and Press Forming, Advanced Studies in Plasticity. Main research interests include advanced mechanical design, manufacturing processes, design of manufacturing systems and statistical process control.